JCTC Journal of Chemical Theory and Computation

Understanding Selectivity of Hard and Soft Metal Cations within Biological Systems Using the Subvalence Concept. 1. Application to Blood Coagulation: Direct Cation−Protein Electronic Effects versus Indirect Interactions through Water Networks

B. de Courcy,[†,‡] L. G. Pedersen,[§] O. Parisel,[†,‡] N. Gresh,[||] B. Silvi,[†,‡] J. Pilmé,[†,‡,⊥] and J.-P. Piquemal*[,†,‡]

UPMC Univ Paris 06, UMR 7616, Laboratoire de Chimie Théorique, case courrier 137, 4 place Jussieu, F-75005, Paris, France, CNRS, UMR 7616, Laboratoire de Chimie Théorique, case courrier 137, 4 place Jussieu, F-75005, Paris, France, Laboratory of Structural Biology, National Institute of Environmental Health, Sciences, Research Triangle Park, North Carolina 27709, Laboratoire de Pharmacochimie Moléculaire et Cellulaire, U648 INSERM, UFR Biomédicale, Université Paris Descartes, 45, rue des Saints-Pères, 75006, Paris, France, Université de Lyon, Université Lyon 1, Faculté de Pharmacie, F-69373 Lyon, Cedex 08, France

Received October 13, 2009

Abstract: Following a previous study by de Courcy et al. (*Interdiscip. Sci. Comput. Life Sci.* **2009**, *1*, 55−60), we demonstrate in this contribution, using quantum chemistry, that metal cations exhibit a specific topological signature in the electron localization of their density interacting with ligands according to their "soft" or "hard" character. Introducing the concept of metal cation subvalence, we show that a metal cation can split its outer-shell density (the so-called subvalent domains or basins) according to it capability to form a partly covalent bond involving charge transfer. Such behavior is investigated by means of several quantum chemical interpretative methods encompasing the topological analysis of the Electron Localization Function (ELF) and Bader's Quantum Theory of Atoms in Molecules (QTAIM) and two energy decomposition analyses (EDA), namely, the Reduced Variational Space (RVS) and Constrained Space Orbital Variations (CSOV) approaches. Further rationalization is performed by computing ELF and QTAIM local properties such as electrostatic distributed moments and local chemical descriptors such as condensed Fukui functions and dual descriptors. These reactivity indexes are computed within the ELF topological analysis in addition to QTAIM offering access to a nonatomic reactivity local index, for example, on lone pairs. We apply this "subvalence" concept to study the cation selectivity in enzymes involved in blood coagulation (GLA domains of three coagulation factors). We show that the calcium ions are clearly able to form partially covalent charge transfer networks between the subdomain of the metal ion and the carboxylate oxygen lone pairs, whereas magnesium does not have such ability. Our analysis also explains the different role of two groups (high affinity and low affinity cation binding sites) present in GLA domains. If the presence of Ca(II) is mandatory in the central "high affinity" region to conserve a proper folding and a charge transfer network, external sites are better stabilized by Mg(II), rather than Ca(II), in agreement with the experiment. The central role of discrete water molecules is also discussed in order to understand the stabilities of the observed X-ray structures of the GLA domain. Indeed, the presence of explicit water molecules generating indirect cation−protein interactions through water networks is shown to be able to reverse the observed electronic selectivity occurring when cations directly interact with the Gla domain without the need of water.

10.1021/ct100089s
Published on Web 03/12/2010

Introduction

Metal cations play a critical role in many biological systems. In most cases, they are specific in their ability to bind to proteins and thereby confer appropriate biological function or activity. For example, the presence of calcium cations is important in blood clotting, signal transduction, and cell division. Specifically, in the case of blood clotting, it has been experimentally observed that the presence of calcium is required for clot formation.[1] Indeed, calcium cations directly participate in the binding and folding of the γ-carboxyglutamic acid (Gla)-rich domain that is common to the vitamin-K-dependent serine proteases present in the blood coagulation cascade.[1] Blood plasma does not coagulate in the sole presence of magnesium ions,[2,3] an effect attributed to the concomitant lack of binding of the Gla residues to negatively charged phospholipids when only magnesium ions are present. More precisely, recent X-ray crystal structures with a mixture of both Ca(II) and Mg(II) show that the N-terminus ω-loop segment that is thought to be the key determinant for the binding of the GLA domain to membranes has a disordered structure when only magnesium ions are present.[4] In the presence of calcium ions, GLA domains have been crystallized and a strong Gla-calcium network has been observed with varying degrees of calcium ion coordination. However, despite the mandatory presence of calcium ions needed to structure the GLA domain and allowing it to point the three hydrophobic (or anionic) residues forming "the keel" in the direction of negatively charged phospholipids found in cellular membranes, it has also been experimentally demonstrated that the presence of magnesium ions in addition to calcium enhances the affinity of the enzyme for both the membrane and cofactors.[5]

The ability of the calcium ion to coordinate water molecules with flexible coordination is thought to be important for this function. At the theoretical level, recent first-principle Car−Parrinello[6] and force-field simulation[7] studies have reported an in-depth description of the hydration shells and of the preferred coordination numbers for the calcium and magnesium cations. Although we know that the residence time for water on a magnesium ion is substantially longer than that for a calcium ion,[8] we as yet do not know the physical origins of the differences between the binding of calcium and magnesium ions in biological systems, as *no clear electron structure−biological activity relation has been uncovered in realistic model systems*. In this context, we proposed to apply modern quantum chemistry to study the nature of the binding of calcium and magnesium ions in model systems of factors VII, IX, and X, the structures of which are based on protein structures extracted from the Protein Data Bank.

Outline

In this work, we will first focus on the fundamental interactions occurring in such systems between the metal cations and their environment. Indeed, thanks to X-ray studies, we know that interactions occur between the calcium or magnesium cations and carboxylate moieties. We will then present an extensive ab initio study of the binding of several hard and soft metal cations to carboxylates in different position. Then, applying quantum topological approaches such as Atoms in Molecules (QTAIM)[9] theory and the topological analysis of the Electron Localization Function (ELF),[10] we shed light on the origin of the different behavior of the electronic structure of metal cation and ligands so as to unravel the specific cation topological signature. The observed topological descriptions will be complemented by intermolecular interaction energy decomposition using the Reduced Variational Space approach (RVS)[11a] and the Constrained-Space Orbital variation (CSOV),[11b] which provide insights about the nature, covalent or electrostatic, of the bonding between the cations and carboxylate. To connect this work to conceptual Density Functional Theory (DFT), we will also provide a detailed analysis by means of local chemical descriptors such as the condensed Fukui functions. In a second part, we will present a study of models of the GLA domain from factors IX, VII, and X of the blood coagulation process using ELF computations complemented by multimolecular RVS energy decomposition analyses.

Method

A. Topological Analysis of ELF. The topological analysis relies on a partition of the molecular space achieved in the framework of the theory of gradient dynamics applied to a scalar potential function, say $V(\mathbf{r})$, called "potential function", which contains the physical or chemical information. This partitioning gives rise to a set of nonoverlapping molecular volumes called basins localized around the maxima of the ELF (the attractors of the vector field). The boundaries between these basins, the separatrices, are zero-flux surfaces satisfying the following condition that every point $\mathbf{r}$ is a unit vector normal to the surface. In the QTAIM theory of Bader,[9] the scalar function is the electron density distribution whose basins have their attractors located on the nuclei and which are therefore associated with the atoms that constitute the molecule. In order to recover a chemist's representation of a molecule consistent with Lewis's valence picture, one must use another "local" function that is able to describe the electron pair regions. For almost two decades, the topological analysis of the ELF has been extensively developed and used to analyze chemical bonding and to investigate chemical reactivity (for reviews, see refs 12 and 13). The ELF can be interpreted as a signature of the electron pair distribution. The relationship of the kernel of ELF to pair functions has been established,[13] but in contrast to these latter, the ELF values are confined in the [0,1] range by a Lorentzian transformation which facilitates the interpretation. The basins

* Corresponding author e-mail: jpp@lct.jussieu.fr.
† UPMC Univ Paris 06.
‡ CNRS, UMR 7616.
§ National Institute of Environmental Health Sciences.
|| Université Paris Descartes.
⊥ Université Lyon 1.

of the ELF are either core basins, labeled C(A) corresponding to the inner shells of atom A and encompassing its nucleus (if $Z > 2$), or valence basins denoted by V(A,B,C...), where A, B, and C are the element symbols. A valence basin can belong to a single atomic valence shell—in this case, V(A) corresponds to a lone pair—or be shared by several atoms and associated to a bond V(A,B).

The ELF basins closely match the electronic domains of the VSEPR[12] model, and it has been shown that the interbasin repulsion provides a map onto the Gillespie−Nyholm rules which describe molecular geometry.[14,15] It has been recently shown that non-VSEPR structures which occur around neutral atoms belonging to the fourth and higher periods can be explained by considering the structure of the external core shell basins[16] and are hereafter referred to as subvalence basins. Details about the ELF analysis can also be found in a recent review paper dealing with the application of ELF to systems of biological interest.[17]

B. Integration of Local Properties within the ELF or QTAIM Partition. *1. Local Electrostatic Moments.* From a quantitative point of view, a population analysis can be carried out by integrating the electron density distribution over the basin volumes. Recently, the distributed moments analysis based on the QTAIM partition[9] and on the ELF basins (DEMEP)[18a] has been introduced, which enables an extended discussion on the nature of bonding in molecules. In this paper, we use more specifically the first moment (denoted as M_1), which represents the local dipolar polarization of the density.

That way, the Distributed Electrostatic Moments based on the ELF Partition (DEMEP) allows the calculation of local moments located at nonatomic centers such as lone pairs, σ bonds, and π systems. Local dipole contributions have been shown to be useful in rationalizing inductive polarization effects and typical hydrogen bond interactions. Moreover, bond quadrupole polarization moments being related to a π character enable a discussion of bond multiplicities and sorting of the families of molecules according to their bond order.

To summarize, the $M_0(\Omega)$ monopole term corresponds to the negative of the population (denoted N):

$$M_0(\Omega) = -\int_\Omega \rho(\mathbf{r})\,\mathrm{d}\tau = -N(\Omega) \tag{1}$$

The first moments or dipolar polarization components of the charge distribution are defined by three-dimensional integrals for a given basin Ω according to

$$\begin{aligned} M_{1,x}(\Omega) &= -\int_\Omega (x - X_c)\rho(\mathbf{r})\,\mathrm{d}\tau \\ M_{1,y}(\Omega) &= -\int_\Omega (y - Y_c)\rho(\mathbf{r})\,\mathrm{d}\tau \\ M_{1,z}(\Omega) &= -\int_\Omega (z - Z_c)\rho(\mathbf{r})\,\mathrm{d}\tau \end{aligned} \tag{2}$$

where X_c, Y_c, and Z_c are the Cartesian coordinates of the basin centers.

The five second-moment spherical tensor components can also be calculated and are defined as the quadrupolar polarization terms. They can be seen as the ELF basin equivalents to the atomic quadrupole moments introduced by Popelier[9c] in the case of an QTAIM analysis:

$$\begin{aligned} M_{2,zz}(\Omega) &= -\frac{1}{2}\int_\Omega [3(z - Z_c)^2 - \mathbf{r}^2]\rho(\mathbf{r})\,\mathrm{d}\tau \\ M_{2,x^2-y^2}(\Omega) &= -\frac{\sqrt{3}}{2}\int_\Omega [(x - X_c)^2 - (y - Y_c^2)]\rho(\mathbf{r})\,\mathrm{d}\tau \\ M_{2,xy}(\Omega) &= -\sqrt{3}\int_\Omega (x - X_c)(y - Y_c)\rho(\mathbf{r})\,\mathrm{d}\tau \\ M_{2,xz}(\Omega) &= -\sqrt{3}\int_\Omega (x - X_c)(z - Z_c)\rho(\mathbf{r})\,\mathrm{d}\tau \\ M_{2,yz}(\Omega) &= -\sqrt{3}\int_\Omega (y - Y_c)(z - Z_c)\rho(\mathbf{r})\,\mathrm{d}\tau \end{aligned} \tag{3}$$

The first- or second-moment basin magnitude is then defined as the square root of the sum of squared components:

$$|\mathbf{M}(\Omega)| = \sqrt{\sum_i M_i(\Omega)^2} \tag{4}$$

Thanks to the invariance of the magnitude of any multipole rank (|M1| or |M2|) with respect to the axis for a given bond or lone pair, the approach allows us to compare the dipolar or quadrupolar polarization of a given basin in different chemical environments.

2. Fukui Functions as Local Chemical Descriptors. Beyond the computations of local distributed electrostatic moments, it is also possible to access the topological partition of local chemical descriptors. Among the numerous chemical indicators, the Fukui functions,[18b,c] based on the relative properties of the Highest Occupied Molecular Orbital (HOMO) and the Lowest Unoccupied Molecular Orbital (LUMO), are interesting as they are particularly useful for the interpretation of chemical reactivity, particularly toward nucleophiles or electrophiles.[18d] Indeed, following Parr and Yang, conceptual DFT provides such functions defined in terms of the variation of the chemical potential with respect to changes in the external potential $v(\mathbf{r})$ or equivalently as the derivative of the electron density with respect to changes in the number of electrons N.

$$f(\mathbf{r}) = \left[\frac{\delta\mu}{\delta v(\mathbf{r})}\right]_N = \left[\frac{\partial\rho(\mathbf{r})}{\partial N}\right]_{v(\mathbf{r})} \tag{5}$$

Three Fukui functions are usually evaluated: $f^+(r)$, $f^-(r)$, and $f^0(r)$

$$\begin{aligned} f^+(\mathbf{r}) &= \left(\frac{\partial\rho(\mathbf{r})}{\partial N}\right)^+_{v(\mathbf{r})} \approx \left(\frac{\delta E_{\mathrm{LUMO}}}{\delta v(\mathbf{r})}\right)_N \approx \rho_{\mathrm{LUMO}}(\mathbf{r}) \\ f^-(\mathbf{r}) &= \left(\frac{\partial\rho(\mathbf{r})}{\partial N}\right)^-_{v(\mathbf{r})} \approx \left(\frac{\delta E_{\mathrm{HOMO}}}{\delta v(\mathbf{r})}\right)_N \approx \rho_{\mathrm{HOMO}}(\mathbf{r}) \\ f^0(\mathbf{r}) &= \frac{1}{2}[f^+(\mathbf{r}) + f^-(\mathbf{r})] \end{aligned} \tag{6}$$

They are sometime also associated with the computation of another value called the dual descriptor (denoted $\Delta f(r)$[18e,f]) and calculated upon the $f^+(r)$ and the $f^-(r)$ functions:

$$\Delta f(\mathbf{r}) = (f^+(\mathbf{r}) - f^-(\mathbf{r}))_N \tag{7}$$

The $f^+(r)$ function usually characterizes the reactivity of a given species toward nucleophilic attack (in that case, $\Delta f(r) > 0$), whereas the $f^-(r)$ function usually characterizes the

reactivity of a given species toward electrophilic attack (in that case, $\Delta f(r) < 0$). When $\Delta f(r) = 0$, the site's reactivity should be equilibrated. As an analytic expression of such function is not available, it remains possible to compute them numerically using finite differences (see for example ref 18g and references therein).

In that case, $f^-(r)$, $f^+(r)$, and $f^0(r)$ can be computed as follows:

$$\begin{aligned} f^-(\mathbf{r}) &= [q_x(N) - q_x(N-1)] \\ f^+(\mathbf{r}) &= [q_x(N+1) - q_x(N)] \\ f^0(\mathbf{r}) &= \frac{1}{2}[f^+(\mathbf{r}) + f^-(\mathbf{r})] \\ \Delta f(\mathbf{r}) &= (f^+(\mathbf{r}) - f^-(\mathbf{r})) \end{aligned} \tag{8}$$

$q_x(N)$ represents the atomic charges associated with atom x within the N-electron species. Recently, it has been shown[18h,i] that it is possible to use a QTAIM condensation scheme for Frontier Molecular Orbitals Fukui functions using finite differences within a topological partition. Such an approach has been shown to be particularly stable, having some advantage on other atomic evaluations of the Fukui functions scheme:

$$\sum_x f_x^\alpha = \sum_x \int_x |\varphi^{h(l)}(\mathbf{r})|^2 \, d\mathbf{r} = \int_x |\varphi^{h(l)}(\mathbf{r})|^2 \, d\mathbf{r} = \int_x f^\alpha \, d\mathbf{r} = 1 \tag{9}$$

where h denotes HOMO, and l, LUMO, and the subscript x under the integration sign indicates that the integration has to be performed only within the particular atomic domain of atom x.

As previouslsy demonstrated for the computations of electrostatic moments, any QTAIM local property computations can be performed using a topological ELF analysis. In this contribution, following the studies by Fuenteabla et al.,[18j] we present a Fukui analysis performed at both QTAIM and ELF levels.

C. Computational Procedures. The geometries of all formate−cation complexes were optimized using the hybrid functional B3LYP[19a,b] with the Jaguar 5.5 software.[20] The choice of the B3LYP functional was motivated by its observed good performance in the modeling of biomolecules containing Ca(II) and Mg(II) cations compared to MP2.[19b,c] We report in Supporting Information S1 some comparisons between different functionals, MP2 and CCSD(T), on optimal Ca(II) (or Mg(II))−formate geometries, confirming these findings. The LACV3P**[21] basis set combining a pseudopotential for the cation, and the all-electron 6-311G** basis set for the other atoms was employed. All geometries obtained with this less accurate energy function were then optimized further using the hybrid functional B3LYP but applying the all-electron 6-311++G** basis set[22] to all atoms, as provided by the Gaussian 03 software.[23] For the coagulation factors studied in the second part of this paper, single point calculations were employed for the two optimized malonate−cation complexes at the B3LYP/6-311++G** level of theory. All topological analyses were carried out using ELF grids of size 180 × 180 × 180 for moment analysis (300 × 300 × 300 for pictures) with the last version of the TopMoD90[24] package coupled to the TopChem[17] program providing DEMEP analysis. To compute the total molecular dipole, we have assumed as "global (or molecular) frame" the standard orientation provided by Gaussian 03, which computes molecular dipoles at the center of nuclear charges. B3LYP/CSOV computations were performed with the same basis set using an in-house version of HONDO 95.3,[25] whereas the GAMESS[26] software provided the RVS results computed at the Hartree−Fock level.

Results

A. Theoretical Description of Hard and Soft Metal-Cation Interactions with Carboxylate Moieties. For blood coagulation proteins, X-ray studies clearly show that the main interactions involved in the biological activity of such enzymes involve networks built on the interaction of calcium or magnesium cations with carboxylate groups.[27] More precisely, X-rays unravel direct malonate−Ca(II)/or Mg(II) interactions.

To start our quantum chemical description of such proteins, we present here results on the interactions of differents metal cations with formate which are simple malonate models. As both monodentate and bidendate formate−cation coordinations are found in the structures, we have investigated the two cases. In a second part, we will focus on the specific interaction of calcium and magnesium cations with more realistic models directly extracted from the PDB structures of the different available factors.

1. Topological Study of Hard and Soft Metal Cations: The Subvalence Concept. In order to study the differences between metal cations, we have performed an ELF analysis upon DFT computations on several metal-cation−formate complexes encompassing monovalent cations such as Li(I), Na(I), K(I), and Cu(I) and divalent cations, namely, Mg(II), Ca(II), and Zn(II). They are displayed in Figure 1a and b. Indeed, in a recent study,[28] we showed that the density of Zn(II) exhibits a striking plasticity. However, Zn(II) binding ligands were shown to be able to adapt/redistribute their density according to their nature: sulfur atoms were shown to be the softest, being able to spatially delocalize their lone pairs, as oxygen and nitrogen mainly contract their lone pair volumes. The present study intends to generalize such observations. Indeed, striking differences can be observed by visually analyzing the obtained ELF topological pictures that can be associated with the well-known Parr and Pearson hardness concept linked to the resistance of an atom to change or deformity. One can see (Figure 1a and b) that the expected "hard cations" (high value of the η_A hardness parameter, see Table 3 of ref 29) such as Li(I), Na(I), or Mg(II) have a spatial localization of their electron density condensed around the nucleus position. "Soft" cations, usually associated with lower η_A values, exhibit specific splits within their outer-shell densities.

It is then possible to use *the concept of a "subvalence"* associated with outer-shell core basins which can be seen as the topological signature for a given hard or soft behavior of the metal. A quick look at the observed topological structures shows that the observed subvalent ELF basins are

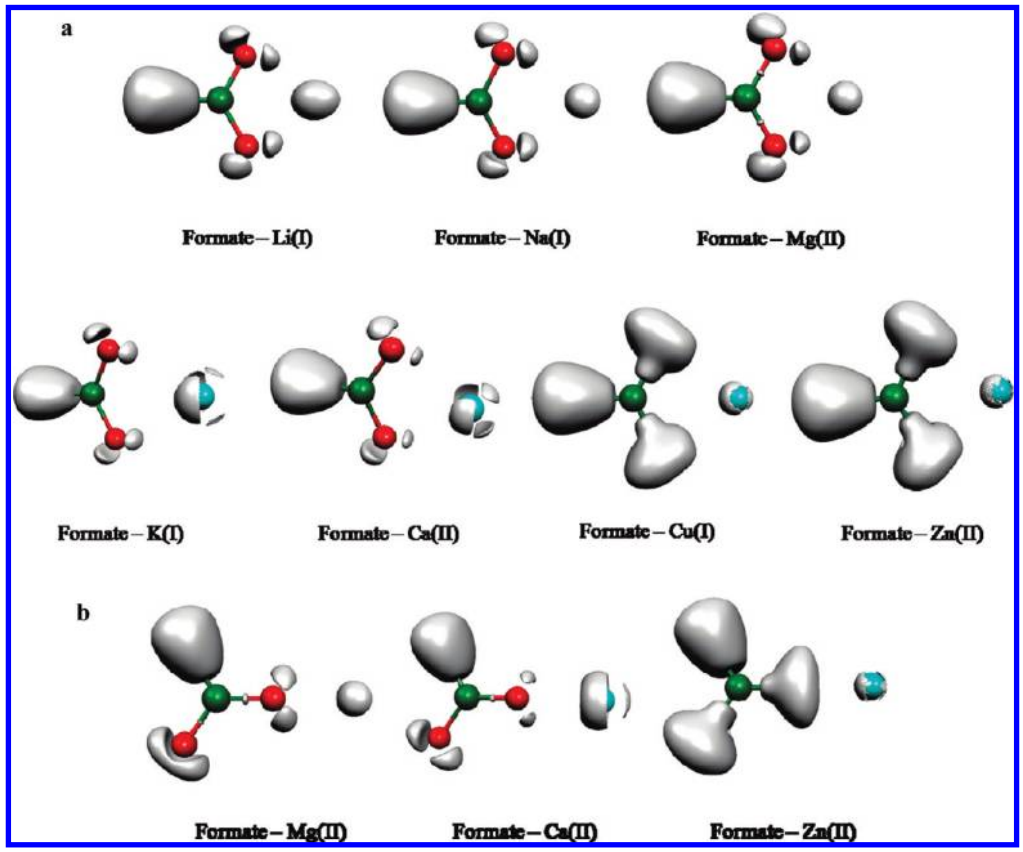

Figure 1. (a) ELF representation of formate interacting in a bidentate mode with metal cations. Topological analysis of interactions between a formate and seven metal cations revealed, at the isosurface, a coefficient of 0.87 (except for Cu(I) and Zn(II) complexes, where it is 0.77). As seen in these pictures, electron densities remain condensed around the nucleus position for hard cations such as Li(I), Na(I), and Mg(II), whereas electron densities are split in four distinct subunits (basins), avoiding oxygen lone pairs, for softer cations such as K(I) and Ca(II), and split in two distinct subunits (basins), one of which is inserted between oxygen lone pairs and the cation, for soft cations such as Cu(I) and Zn(II). In soft cation complexes, a blue sphere describes the core electrons of the cations. In hard cation complexes, the spherical subvalence obscures the core electrons so that the blue sphere is not visible. (b) ELF representation of formate interacting in a monodentate mode with metal cations. Isosurface coefficients used to make theses pictures are the same as the ones used for part a. A very similar pattern is observed as for the bidentate formate−cation complexes. The Mg(II) electron density stays spherical. In the Ca(II) complex, three basins have merged into an annular one still avoiding oxygen lone pairs. The same split as for the bidentate complex is shown for Zn(II).

more numerous for soft cations, reflecting a more covalent character of their bonding to formate anions (see Figure 1).

2. Subvalence: Understanding Physics at Play. To have a deeper understanding of the physics taking place in such interactions, it is possible to extend the ELF analysis to the computation of local electrostatic moments (see Table 1) and Fukui functions (see Table 3) and to correlate them to RVS energy decompositions (see Table 2).

From these tables, we see that the more covalent the bonding character of the formate−cation intermolecular bond is, the greater the RVS cation polarization energy and local ELF cation dipole moment are. For example, a hard cation such as Na(I), which is poorly polarizable (weak polarizability), is involved in interactions dominated by electrostatics (Table 2) and does not show any split within its subvalence, whereas cations exhibiting stronger polarization and charge transfer interactions possess a higher number of basins. Moreover, for a covalently bonded very soft cation such as Zn(II), a subvalent Zn−O basin is observed between the formate oxygen lone pair and the metal, a hint of electron sharing. Ca(II), which is less soft and less covalently bonded, still exhibits a split, but subvalent basins remain distributed around the nucleus (Figure 1) and do not form any bond. Correlated CSOV energy decomposition computations have also been performed and are fully in line with HF RVS results. Details can be found in the Supporting Information, S2.

Observations of both monodentate and bidentate coordination modes show that "soft cation" subvalent basins clearly have the ability to orient themselves toward the formate oxygen lone pairs. That way, depending on its electron structure, each cation shows a specific topological signature which enables one to predict specific abilities of the cation to interact with its immediate environment thanks to the plasticity of its valence electron spatial organization. An indirect measurement of the soft/hard nature of the cations can be appraised by studying the volumes and density values of the formate oxygen lone pairs when interacting with cations. Hard cations such as Li(I) or Mg(II) clearly act on the lone pair densities which appear lower when compared to softer cations. Figure 2 exhibits the four oxygen lone pairs as they are when no metal cation interacts with the formate. Volume and density values reveal a dissymmetry between the internal and the external lone pairs, internal ones being

Table 1. QTAIM and ELF M_1 and Dipole Moments of Formate−Cation Complexes[a]

		M_1			μ(D)		
		QTAIM	ELF		−QTAIM	ELF	
		Ω(M)	C(M)	V(M)			ab initio
formate Li					0.92	0.90	
	mono	0.01	0		9.41	9.40	9.39
	bi	0	0		3.95	3.95	3.96
Na							
	mono	0	0.07		11.60	11.67	11.69
	bi	0	0.08		6.03	6.06	6.07
K							
	mono	0.21	0.31		12.50	12.60	12.70
	bi	0.20	0.31		7.20	7.30	7.30
Mg							
	mono	0.15	0.06	0.19	13.30	13.30	13.30
	bi	0.02	0.06		7.30	7.30	7.30
Ca							
	mono	0.19	0.37		14.80	14.90	14.90
	bi	0.16	0.35		8.06	8.10	8.11
Cu							
	mono	0.18	0.47		8.08	8.10	8.13
	bi	0.23	0.48		2.97	3.01	3.04
Zn							
	mono	0.23	0.36	0.45	6.41	6.44	6.45
	bi	0.04	0.39		3.06	3.09	3.10

[a] Values of cation's M_1 and dipole moment (μ expressed in Debye) for formate−cation complexes in both modentate (mono) and bidentate (bi) binding modes. M_1 is the polarization component of the total dipole moment (see text and Supporting Information). Concerning a cation, it is computed as the gap to the sphericity: the more a cation exhibits a spherical subvalence, the less its polarization and M_1 value are and vice versa. Two sets of M1 are reported: QTAIM values where all the electrons are gathered around the nucleus Ω(M) and ELF values where electrons are spread over the core basin C(M) and the subvalence basin V(M). QTAIM and ELF values for the total dipole moment are also reported; ab-initio dipole moments computed with Gaussian G03 software are given for comparison.

less populated and more contracted than the external ones. This is due to the fact that the internal lone pairs interact with each other because of the shorter distance between them. From Figures 1 and 2, it is possible to appraise the electronic redistribution within the oxygen lone pairs according to the presence or not of a binding metal cation and to its hardness or softness. Overall, it is important to point out that trends are conserved between ELF observations and Parr's hardness concept.[29] However, ELF pictures the final state of the cation electronic structure within the complex after cation−ligand orbital mixing and metal density relaxation (therefore, a feature also linked to its polarizability).

Concerning the specific Ca(II)/Mg(II) differences, our results demonstrate that overall less flexibility occurs in Mg(II) density compared to Ca(II), which tends to adjust to its immediate ligands. However, for Mg(II) in the monodentate binding mode, a slight increase of cation polarization associated with a topological split of its outer-shell density is noted, and this leads to the fact that Mg(II) could act slightly differently from usual hard cations. As we will see, this will have some consequences. Figure 3 shows a ELF representation of both monodentate and bidentate formate−Mg(II) complexes. A well-separated additional basin is found in the monodentate complex, where a partial charge is transferred. It worth noting that the Sr(II) cation which is sometimes found to substitute calcium under certain conditions (ref 30 and references therein) exhibits the same topological pattern as Ca(II).

To conclude, as the concepts of softness and hardness are involved, it is of importance to also consider the possibility of computing other popular local reactivity indicators, usually utilized to rationalize such phenomena. That way, we propose here an evaluation of the different "local" Fukui functions at both QTAIM and ELF levels. First, we computed such functions on an isolated formate molecule (see Table 3a and b). Again, the ELF Fukui analysis clearly shows the nonequivalence of the formate

Table 2. RVS Energy Components for Selected Formate−Metal Cation Complexes[a]

kcal/mol		elec.	exch.	E1	Epol	Epol(cation)	ECT	E2	Etot
formate Li(I)									
	mono	−158.3	27.8	**−130.4**	−17.6	**−0.2**	−4.5	**−22.1**	−152.6
	bi	−179.2	28.1	**−151.1**	−14.5	**−0.1**	−6.7	**−21.2**	−172.3
formate Na(I)									
	mono	−138.0	20.9	**−117.1**	−10.1	**−0.3**	−0.2	**−10.3**	−127.4
	bi	−159.2	22.7	**−136.5**	−8.3	**−0.2**	−1.0	**−9.3**	−145.8
formate K(I)									
	mono	−125.9	26.4	**−99.5**	−8.7	**−1.8**	−1.3	**−9.9**	−109.5
	bi	−147.0	30.2	**−116.8**	−7.1	**−1.7**	−1.6	**−8.6**	−125.4
formate Mg(II)									
	mono	−300.0	43.7	**−256.3**	−54.4	**−0.4**	−7.8	**−62.1**	−318.4
	bi	−354.7	52.7	**−302.0**	−48.4	**−0.3**	−15.8	**−64.1**	−366.1
formate Ca(II)									
	mono	−287.7	76.3	**−211.5**	−39.8	**−2.3**	−17.8	**−57.7**	−269.1
	bi	−335.9	82.4	**−253.5**	−32.8	**−2.0**	−18.4	**−51.2**	−304.7
formate Cu(I)									
	mono	−177.6	68.1	**−109.5**	−29.3	**−15.3**	8.4	**−20.9**	−130.4
	bi	−186.9	50.7	**−136.2**	−19.1	**−8.1**	3.3	**−15.8**	−152.1
formate Zn(I)									
	mono	−319.5	66.7	**−252.8**	−64.9	**−4.5**	−6.7	**−71.6**	−324.4
	bi	−371.0	72.1	**−298.9**	−56.0	**−3.4**	−18.8	**−74.8**	−373.7

[a] Values are given for the two monodentate (mono) and bidentate (bi) cation binding modes. elec. is the Coulomb electrostatic energy; exch. is the exchange repulsion. The sum of the two constitutes the first-order term E1. Epol and ECT are the polarization and charge transfer components of the second-order term E2, Etot being the sum of E1 and E2. An RVS decomposition energy allows us to separate the second-order terms over the constitutive fragments of a system. The individual polarization of each cation is reported. The more spherical the subvalence of a cation is, the less Epol is. The same pattern is observed for the ECT of each complex. It can be seen that ECT for the monodentate formate−Mg(II) complex is double that of the bidentate formate−Mg(II) complex. This is to be put in context with the appearance of the additional subvalence basin in the monodentate formate−Mg(II) complex (Figure 3).

Table 3. (a) ELF Integrated Fukui Functions and Dual Descriptor Values for an Isolated Formate Molecule, (b) QTAIM Integrated Fukui Functions and Dual Descriptor Values for an Isolated Formate Molecule, (c) ELF and QTAIM Fukui Functions and Dual Descriptor Values for Selected Metal Cations[a]

	part a			
formate basin	f^-(ELF)	f^+(ELF)	f^0(ELF)	Δf(ELF)
C(C)	0.00	0.00	0.00	0.00
C(O1)	0.02	0.00	0.01	0.02
C(O2)	0.02	0.00	0.01	0.02
V(C,H)	0.22	0.30	0.26	−0.08
V(C,O2)	0.04	0.01	0.02	0.03
V(C,O1)	0.04	0.01	0.02	0.03
V(O1)	0.20	0.01	0.10	0.19
V(O1)	0.13	0.03	0.08	0.10
V(O2)	0.14	0.03	0.09	0.11
V(O2)	0.20	0.01	0.10	0.19

	part b			
formate atom	f^-(QTAIM)	f^+(QTAIM)	f^0(QTAIM)	Δf(QTAIM)
H	0.17	0.15	0.16	0.02
C	0.05	0.04	0.05	0.02
O_1	0.38	0.03	0.21	0.35
O_2	0.38	0.03	0.21	0.35

	part c						
cations	f^-(QTAIM)	f^+(QTAIM)	f^0(QTAIM)	Δf(QTAIM), isolated	Δf(ELF), isolated	Δf(QTAIM), complexed	Δf(ELF), complexed
Li	1.00	0.23	0.61	0.77	0.70	−0.14	−0.11
Na	1.00	0.44	0.72	0.56	0.45	−0.34	−0.37
K	1.00	0.46	0.73	0.54	0.43	−0.30	−0.36
Mg	1.00	0.59	0.79	0.41	0.32	−0.67	−0.24
Ca	1.00	0.98	0.99	0.02	0.00	−0.55	−0.59
Zn	1.00	0.91	0.96	0.09	0.04	−0.69	−0.50

[a] Values are given for the isolated cations and for a cation within a bidentate formate−metal complex.

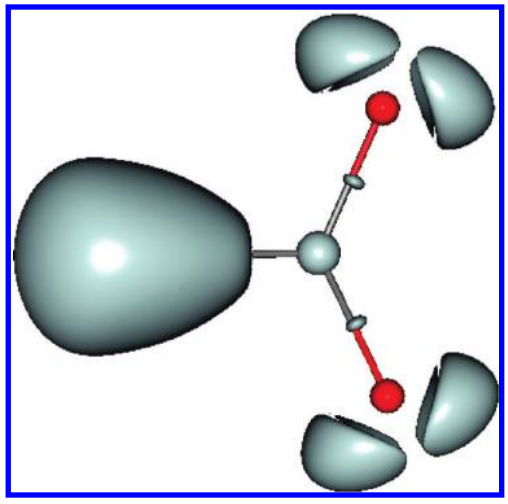

Figure 2. ELF representation of a formate without a binding cation. This picture presents a formate in an uncomplexed state, where densities are not rearranged through interactions with a cation. Volumes of the oxygen lone pairs can be compared to the ones of formate−cation complexes shown in Figure 1a and b.

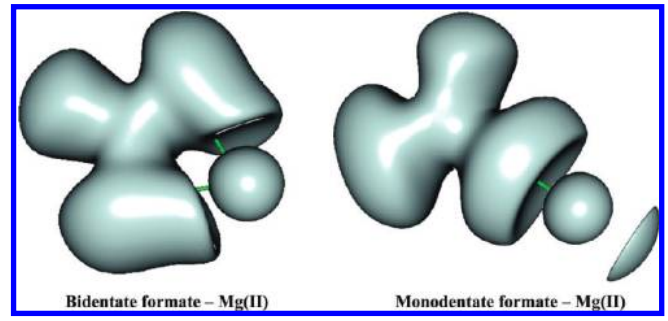

Figure 3. ELF representation of formate−Mg(II) complexes at an isosurface coefficient of 0.22. The electron density of the two formate−Mg(II) complexes are compared in this picture. Contrary to the bidentate formate−Mg(II), where the subvalence stays spherical, in the monodentate formate−Mg(II), an additional basin appears at the opposite side of the coordination to the oxygen. This is consistent with the augmentation of both M_1 shown in Table 1 and charge transfer energy shown in Table 2 for this complex.

oxygen lone pairs, the external basins having different indicators from internal lone pairs. If QTAIM tends to show a uniform Fukui descriptor (the dual descriptor Δf is always positive), ELF does not, as it provides a Δf negative value on the C−H bond, providing insight about a possible different reactivity.

Concerning the metal cations, Table 3c brings interesting information. Let us first consider first the isolated metal cations. If all cations exhibit f^- values of 1, they have very different f^+ values. Again, following chemical intuition, strong differences occur between hard and soft cations. Hard cations such as Li(I) exhibit low values of f^+, whereas soft cations such as Zn(II) have f^+ values tending toward 1. The dual descriptor appears then to be a good global indicator reflecting the cation's ranking as Δf tends to 0 with increasing

cation softness. Table 3c depicts the results for selected bidentate formate cations. Global trends are preserved despite strong, different bonding modes. Again, the softer cations exhibit smaller Δf values (here more negative) than harder ones. If they agree well, one difference between ELF and QTAIM values is observed: ELF tend to show more difference between Ca(II) and Mg(II) than QTAIM. This is reflected by a difference of 0.2 (QTAIM) vs 0.3 (ELF) in the Δf values between the two cations.

Of course, the numerical values strongly depend on the (never unique) topological partition scheme and therefore on the density attribution to atoms/centers,[18h] but the ELF and AIM approaches are not subject to strong basis set/diffuse function dependence[18a,h] and are quite stable. Overall, beyond the numbers, an interesting qualitative agreement is observed and supports the previously depicted ELF subvalence basins and the numerical values extracted from other interpretative techniques described above.

B. Metal Cation's Electron Structure/Biological Activity Relationship in Coagulation Proteins. We use here the commonly accepted terminology, first, to differentiate the γ-carboxyglutamic acid itself, identified as Gla, from the γ-carboxyglutamic acid-rich domain, identified as GLA, second, to name the first 11 residues at the N-terminal extremity of the ω-loop, and third to specifically identify residues 4, 5, and 8 (5, 6, and 9 for FIX) from the previous sequence as the keel. In addition, since we have to compare several GLA domain crystal structures, each having their Ca(II) or Mg(II) positions differently numbered, we will use for clarity purposes the same numbering for all, that is, the one found in the crystal structure of the human factor VII (1DAN, see ref 38).

1. Metal Cation's Electron Structure/Biological Activity Relationship in Coagulation Proteins. When a blood vessel is injured, a cascade of protein−protein interactions[1] rapidly occurs, leading to the formation of a cross-linked fibrin clot, eventually restoring the integrity of the circulatory system. A number of proteins involved at the early stage of the process are vitamin-K-dependent zymogens of serine proteases.[31] Among this family of coagulation factors, factor VII, once activated and bound to tissue factor (TF), activates zymogen factors IX and X into functional factors IXa and Xa. These in turn transform prothrombin into active thrombin, which is ultimately responsible for the conversion of fibrinogen to fibrin.[32] A cell-based model of coagulation, which incorporates the important roles of endothelial cells and platelets, has recently been introduced, and this more physiological view appears to be gaining acceptance.[33] Many other factors and cofactors are necessary for the completion of the mechanism, but we will focus only on two steps.[1]

2. Structural Analysis and Biological Activity. The above-mentioned three factors are made up by four domains. At the N extremity, we find a GLA domain, followed by two Epidermal Growth Factor (EGF) like domains, namely, EGF1 and EGF2, terminated by a Serine Protease (SP) domain. The primary structures of GLA domains (residues 1 to 48) are highly conserved:[34] only a few residues differ along the sequences of factors VII, IX, and X. Remarkably, the first nine Gla residues, as well as two cysteines, are always found precisely at the same place. Accordingly, for all factors, two hydrophobic residues are adjacent to the first group of two Gla residues: Phe4 and Leu5 for FVIIa and FXa factors and Leu6 and Phe9 for FIXa. We can also notice the presence of an Asn residue in the second position of the sequence. Moreover, analysis of the PDB files for these factors shows that the secondary structures are also very similar and essentially superimposable. From the N extremity to the end of the domain, we find successively the ω-loop with its two above-mentioned hydrophobic amino acids along with either another hydrophobic residue (FVIIa−Leu8 and FXa−Met8) or a cationic one (FIXa−Lys6) pointing their side chains toward the exterior of the protein. Three α-helices are also found. The first two are parallel and maintained so by a disulfide bridge established by the two cysteines cited before. All Gla residues are distributed along these three subunits: Gla6 and -7 are at the top of the central loop of the ω-loop; Gla14, -16, -19, and 20 belong to the first α helix, whereas Gla25, -26, and -29 belong to the second. The third α-helix links the GLA domain to the remaining part (3rd helix) of the protein. A Gla residue can also be found in this part of the domain. In all examined X-ray structures, eight cations are present.[38] One cation is located at the hinge between the third α helix and the first chain of the EGF1 domain. The other seven cations are found aligned at the interstice between the base of the two parallel α helices and the top of the ω-loop. In this zone, two groups of cation binding sites can be defined. The first group is called "high affinity" Ca(II) binding sites[39] and is constituted by the 5 inner Ca(II) sites (numbered 3, 4, 5, 6, and 8, respectively).[38] Within these sites, Ca(II) were found coordinated 6, 7, 7, 7, and 3 times, respectively, at distances in the 2.4−2.8 Å range in the very first GLA domain ever structurally determined (1992), namely, the GLA domain of Ca−Prothrombin Fragment I (see Figure 4 and Table 3 of ref 35). Subsequently, several authors[36,37,41] reported very similar coordination numbers and distances for the factors studied here. The second group, called "low affinity" Ca(II) binding sites, defines the two external sites. At these positions, cations can be either Ca(II) or Mg(II). Figure 4 lists the cation binding sites present in different PDB structures of the studied factors' GLA domains. Occupation by either Ca(II) or Mg(II) in all binding sites seems to be due to details in the preparation of the protein crystal during the X-ray crystallization process. In fact, F VIIa (1DAN),[38] F IXa (1J35),[39] and F Xa (1IOD)[40] were prepared using only $CaCl_2$ as crystallographic salt. It is noticeable that all the binding sites are occupied by calcium, solely present in the environment. When $MgCl_2$ is added to $CaCl_2$, at physiological concentration, for the preparation of F IXa (1J34),[39] all the inner binding sites are occupied by calcium, while the external binding sites are occupied by magnesium. But, prepared under the same conditions, a recent X-ray structure deposited in the Protein Data Bank by Bajaj et al. shows Mg(II) residing in the central site number 5 replacing Ca(II) in the GLA domain of F VIIa (2A2Q).[41] However, when only $MgCl_2$ is used for the preparation of F Xa (1P0S),[4] the two external sites contain a Mg(II) cation, but the sole central site number 5 shows a third Mg(II) cation. In addition, contrary to the five other

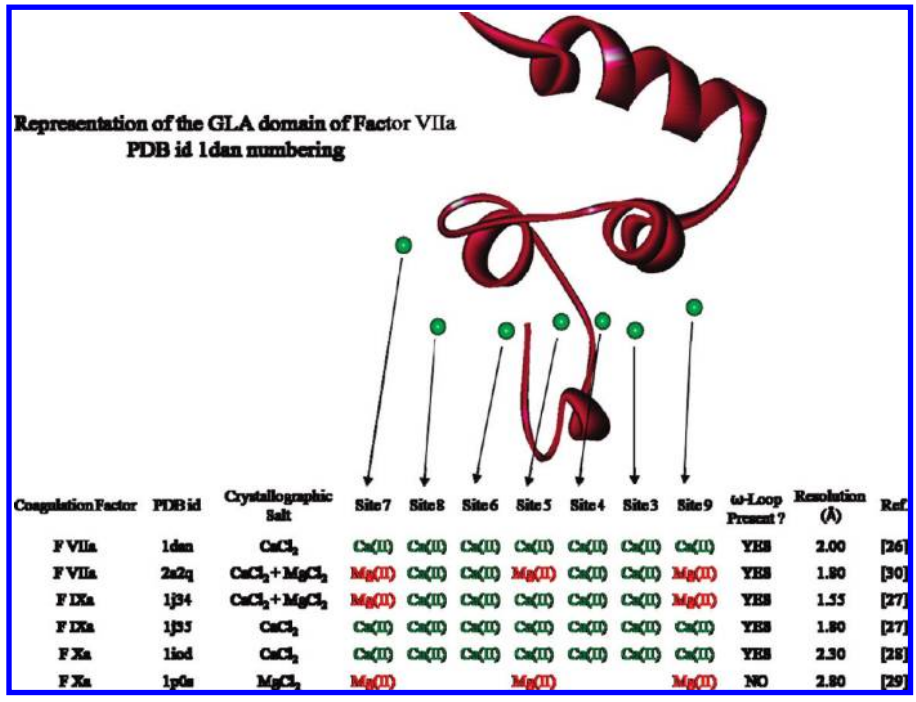

Coagulation Factor	PDB id	Crystallographic Salt	Site 7	Site 8	Site 6	Site 5	Site 4	Site 3	Site 9	ω-Loop Present ?	Resolution (Å)	Ref.
F VIIa	1dan	$CaCl_2$	Ca(II)	Ca(II)	Ca(II)	Ca(II)	Ca(II)	Ca(II)	Ca(II)	YES	2.00	[26]
F VIIa	2a2q	$CaCl_2$+$MgCl_2$	Mg(II)	Ca(II)	Ca(II)	Mg(II)	Ca(II)	Ca(II)	Mg(II)	YES	1.80	[30]
F IXa	1j34	$CaCl_2$+$MgCl_2$	Mg(II)	Ca(II)	Ca(II)	Ca(II)	Ca(II)	Ca(II)	Mg(II)	YES	1.55	[27]
F IXa	1j35	$CaCl_2$	Ca(II)	Ca(II)	Ca(II)	Ca(II)	Ca(II)	Ca(II)	Ca(II)	YES	1.80	[27]
F Xa	1iod	$CaCl_2$	Ca(II)	Ca(II)	Ca(II)	Ca(II)	Ca(II)	Ca(II)	Ca(II)	YES	2.30	[28]
F Xa	1p0s	$MgCl_2$	Mg(II)			Mg(II)			Mg(II)	NO	2.80	[29]

Figure 4. Description of metal cation coordination sites of six GLA domains. The picture is a representation of the GLA domain of F VIIa (1DAN), exhibiting its constitutive parts including the seven cation binding sites. For each site, a comparison of six X-ray geometries shows its occupation by either a Mg(II) or a Ca(II) cation, according to the crystallographic salt used for the preparation.

structures that contain it, no ω-loop is present in the structure of this domain, its constitutive peptide seeming to "float" in the environment. From these observations, it may be deducted that Ca(II) cations are necessary in the central zone to structure the ω-loop and that the external sites are usually occupied by magnesium. Close examination of the binding of the ω-loop to the rest of the GLA domain reveals the network of interactions between the amino acids borne by the ω-loop, the cations and the amino acids present in the two antiparallel α helices. In all factors where the ω-loop is present, except for F VIIa with Mg(II) in the central site, the NH_3^+ extremity of Ala1 (or Tyr1 for F IXa) establishes three H bonds with the surrounding residues, namely, carbonyl O of Gln21 (F VIIa), Ala21 (F Xa), or Lys22 (F IXa); Oϵ_4 of Gla20 (F VIIa and F Xa) or Gla21 (F IXa); and Oϵ_4 of Gla26 (F VIIa and F Xa) or Gla27 (F IXa). In F VIIa (2A2Q), however, a single H-bond remains with Oϵ_2 of Gla26. A comparison between coordination numbers and coordination distances for each cation of the two structures of F VIIa (1DAN vs 2A2Q), as given in Table 2 of ref 41 by Bajaj et al., reveals that, when only Ca(II) is present in the five inner sites, direct coordinations of cations by the carbonyl O of Ala1 (or Tyr1 for F IXa); Oδ_1 of Asn2; Oϵ_1 and Oϵ_4 of Gla6; and Oϵ_1, Oϵ_2, and Oϵ_4 of Gla7 are observed. By contrast, in F VIIa (2A2Q), where the central Ca(II) is substituted by Mg(II) with two water molecules (S209 and S363) completing the coordination sphere of this cation, the same interactions are observed, but this time through a network of eight water molecules (S209, S262, S363, S411, S508, S602, S694, and S722), present in between the cations and the ω-loop. As a consequence, the ω-loop has moved down approximately 0.5 Å in order to leave enough space for water to insert (see Figure 2A of ref 41).

The existence of the ω-loop is of much importance in that the very first step of the coagulation process is for coagulation factors to colocalize on cell surfaces.[42] In that step, the biological function of the GLA domain is first directly responsible for the linkage of the factors to the membranes, and ultimately to the fibrin clot. This can be done thanks to the three hydrophobic residues of the ω-loop[43] (or two hydrophobic residues and a cationic one in F IXa), oriented in such a way that they are able to dive deeply inside the membrane and interact through hydrophobic bonds with neighboring lipids,[43,44] in addition probably through a buried salt bridge involving Lys5 of F IXa.[43] The deep insertion of the GLA domain inside the membrane also allows the creation of an interaction between a phosphatidylserine (PS) of the membrane and the Ca(II) cation present in binding site number 8, strengthening the anchorage of the coagulation factor inside the cellular membrane.[45] Inhibition of the GLA domain by direct ligand bonding to the ω-loop (such as snake venom protein, see ref 39) is responsible for the loss of membrane linking with a subsequent loss of the coagulation process.

3. Theoretical Study of Interactions of Ca(II) vs Mg(II) with Malonate Groups. In this section, we systematically supplement the ELF analysis with detailed RVS energy decomposition results.

In GLA domains, the transformation of glutamic acids in Gla is realized by the action of vitamin K and several specific enzymes with the addition of a carboxylate group to the γ-carbon of the glutamate;[46] two carboxylate groups borne by the same γ carbon constitutes a malonate group. Two malonates coordinating a metal cation is one of the unit structures observed in GLA domains, displaying as many as four monodentate formate−cation interactions. Two

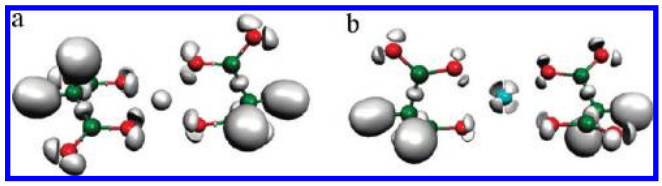

Figure 5. (a) Optimized geometry of a two-malonate−Mg(II) complex. (b) Optimized geometry of a two-malonate−Ca(II) complex. All the ELF pictures were revealed at the 0.87 isosurface coefficient. These pictures exhibit the perfect tetrahedral binding mode of the cations. Mg(II) subvalence is spherical, and the Ca(II) one is split in four well separated basins recalling the bidentate formate−cation complexes.

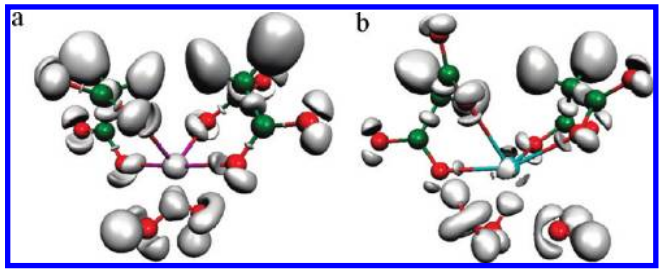

Figure 6. (a) Extracted two-malonate−Mg(II) "deformed tetrahedral" complex. (b) Extracted two-malonate−Ca(II) "deformed tetrahedral" complex. The Mg(II) complex is binding site no. 7 of F IXa (1J34); the Ca(II) one is binding site no. 9 of F Xa (1IOD). Water molecules complete the coordination sphere of each cation: six for Mg(II) and seven for Ca(II). Cation coordinations are also disclosed in order to evidence the "deformed tetrahedral" binding mode of the cations. Each cation behavior does not change as the number of coordinations increases.

different computations at the same level of theory (B3LYP/6-311++G**) have been performed on these systems: a single point calculation using directly extracted geometries from PDB structures on which H atoms were added and geometry optimizations performed using the previous systems as starting points. At the end of the optimization process, the obtained complexes show the two approximate planes of malonates perpendicular to each other around the metal cation, itself four times tetrahedrally coordinated with coordination distances of approximately 2.1 Å for the magnesium and 2.4 Å for the calcium. A calcium complex was extracted from the PDB structure of F Xa (1IOD), whereas the magnesium complex was extracted from the PDB structure of F IXa (1J34). From these two systems, external binding sites (number 7 or 9) are selected, in which cations are surrounded by solvating water molecules: two for Mg(II) and three for Ca(II). Figures 5a and b show the ELF topological analysis on the two optimized geometries. As expected, Mg(II) (Figure 5a) does not exhibit any split of its subvalence, whereas Ca(II) (Figure 5b) has its subvalence split into four well separated basins, oriented in such a manner that no oxygen lone pair faces a cation basin. The same pattern as described above is observed in Figure 6a for Mg(II) and Figure 6b for Ca(II), within the extracted geometries. Thus, upon increasing the coordination number from two in the bidentate formate−cation complexes to four in the optimized geometries shown in Figures 5a and b and ultimately to their maximum in the extracted complexes, each cation consistently exhibits the same behavior. Table 4 reports the results of the RVS analysis, disclosing the individual contributions of the interaction energies for the two malonate−cation complexes shown in Figures 5a and b and 6a and b. These results show first a greater electrostatic term for Mg(II) less compensated by the repulsion term than for Ca(II). As a result, the excess of electrostatic energy reflected by the negative first order term of Mg(II) over Ca(II) is −90 kcal/mol for the optimized complexes and less than −77 kcal/mol for the extracted geometries, reflecting the hardness of the Mg(II) cation. Since a RVS analysis can separate the second order energies for each constitutive monomer of a many-body system, the individual polarization energies of the cations are also reported. It can thus be observed that, as Ca(II) moves away from its optimal geometry, its polarization increases, and that Mg(II) is essentially not polarized. The charge transfer contribution in the Ca(II) complexes decreases upon moving away from the optimal geometry but remains significant, whereas it is null for the Mg(II) optimized complex and slightly increases in the

Table 4. Theoretical RVS Analysis of Tetrahedral Cation Binding Sites[a]

kcal/mol	2 malonates + Mg(II)	2 malonates + Mg(II)	2 malonates + Ca(II)	2 malonates + Ca(II)
geometry	optimized	F IXa 1J34	optimized	F Xa 1IOD
figure number	5a	6a	5b	6b
electrostatic	−777.7	−703.3	−709.0	−636.8
repulsion	90.8	68.2	111.5	78.2
first order energies (e_1)	−686.9	−635.1	−597.5	−558.6
polarization of cations	**−0.1**	**−0.3**	**−0.6**	**−2.2**
polarization	−94.2	−90.5	−63.0	−61.5
charge transfer	0.0	−1.4	−11.2	−9.7
second order energies (e_2)	−94.2	−91.9	−74.2	−71.2
total $e_1 + e_2$	−781.1	−720.9	−671.7	−629.8

[a] RVS energy decomposition has been performed upon theoretical models of tetrahedral binding sites. They are built on the same number of atoms (no water molecules are considered) in order to directly compare the energy contributions. Optimized geometries are the extracted ones on which the optimization process was performed. Mg(II) complexes' first order terms are greater than the ones of Ca(II) complexes, whereas Ca(II) cations are more polarized and generate a larger charge transfer than for Mg(II). This is consistent with the Mg(II) cation having a spherical subvalence entering in more electrostatic types of interactions and the Ca(II) cation splitting its subvalence and creating more interactions of covalent type.

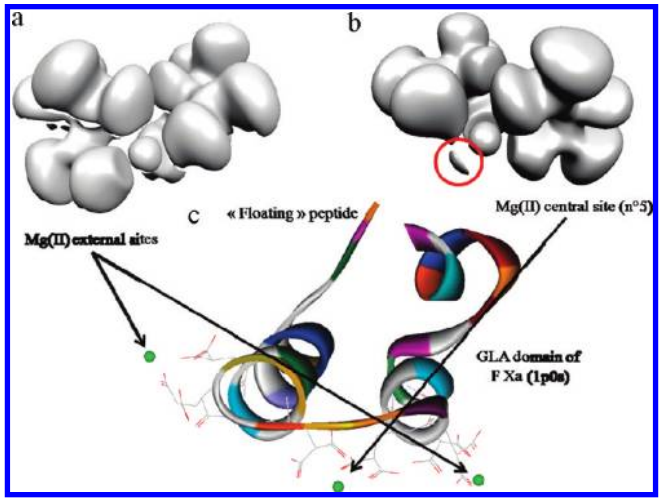

Figure 7. (a) "Hard" Mg(II) binding mode. (b) "Soft" Mg(II) binding mode. (c) Localization of the two binding modes within F Xa (1P0S). Electron densities are revealed at the isosurface coefficient of 0.22. The additional basin shown in the red circle is confirmed by the increase of the charge transfer energy illustrated in Table 4 (−7.6 kcal/mol). As is the case when only Mg(II) is present in a vitamin-K-dependent coagulation factor environment, the cations occupy only the three tetrahedral binding sites, being unable to structure the ω-loop, and leaving its constitutive peptide floating.

complex extracted from X-ray crystallography. It can be deduced that, contrary to Mg(II), Ca(II) is polarized as it is in the bidentate formate−cation type of complex and that the charge transfer contribution becomes selective from one cation to another in such complexes. Thus, Mg(II) enters a more electrostatic interaction, whereas a polarized Ca(II), generating a stronger charge transfer, enters a more covalent interaction. It is important to point out that we also perform such analysis in the presence of an additional PCM implicit solvent. We did not observe any changes in the topology of the system. Such results can be found in Supporting Information S3.

4. Theoretical Study of the Selectivity Ca(II)/Mg(II). a. Is the Mg(II) Cation Strictly Hard in the Gas Phase? In the GLA domain of F Xa (1P0S), in which only magnesium ions are present in the environment, a Mg(II) is observed to be three times coordinated to oxygen atoms of Gla 16 and 26, in the 2.3−2.5 range of distances. Figures 7a and b compare the topology of Mg(II) in two positions: the first one (Figure 7a) comes from an external cation site (site no. 7 of F IXa 1J34); the second one (Figure 7b) is the central site (no. 5). Due to the low resolution (2.8 Å) of the crystal structure of F Xa (1P0S), no water molecule is resolved near the cation in the central site no. 5. Despite the fact that water must be present within the coordination sphere of Mg(II) in a real enzyme, no water molecule is considered in the present theoretical gas phase study, so that the coordination number is four for the external site and three for the central site. As can be seen in Figure 7a, the cation does not exhibit any split of its subvalence, whereas in Figure 7b, the presence of the additional basin (red circle), recalling the monodentate formate−Mg(II) binding mode, clearly suggests that Mg(II) transfers a part of its density into this additional basin. This is confirmed by the magnitude of the RVS charge transfer contribution (see FXa 1P0S in Table 5), namely, −7.6 kcal/mol, instead of a null charge transfer in the optimized geometry. In this particular case, it is important to point out that Mg(II) does not have a hard cation behavior since it exhibits some subvalence capabilities. However, if such a finding is important for understanding the electronic distribution in Mg(II) complexes, could it have an impact when considering more realistic condensed phase GLA domains containing explicit solvent molecules?

b. Selectivity of Ca(II) vs Mg(II) Cations within the Six Gla Domains. From Figure 4, we have found three possible binding sites for Mg(II), namely, sites no. 7 and 9 (external) and 5 (central), the latter exhibiting either a Mg(II) or a Ca(II). The other sites are exclusively occupied by Ca(II) cations, a necessity to structure the ω-loop in its functional geometry. These observations have been confirmed by several experiments, in which Mg(II) and Ca(II) were added at physiological concentration to a previously divalent cation-free environment.[2] When only Mg(II) is present, no enzymatic activity occurs. This is to be put in relation with the

Table 5. RVS Analysis of Selected Cation Binding Sites, Extracted from X-Ray Structures[a]

kcal/mol	2 malonates + Mg(II)	2 malonates + Mg(II)	Mg(II) hexa coordinated	2 malonates + Ca(II)	Ca(II) octa coordinated
Water molecules	**2**	**0**	**3**	**3**	**2**
PDB ID	F IXa 1J34	F Xa 1P0S	F VIIa 2A2Q	F Xa 1IOD	F IXa 1J34
figure number	6a	7b	8a	6b	8b
electrostatic	−696.7	−577.9	−746.5	−690.6	−598.5
repulsion	130.0	23.7	184.5	188.3	111.1
first order energies (e_1)	−566.7	−554.3	−562.0	−502.3	−487.4
polarization of cations	**−0.4**	**−0.4**	**−0.1**	**−1.8**	**−0.5**
polarization	−122.8	−66.5	−92.6	−95.0	−33.0
charge transfer	−9.8	−7.6	−2.7	−20.7	−4.9
second order energies (e_2)	−132.5	−74.1	−95.3	−115.7	−37.9
total $e_1 + e_2$	−699.2	−628.4	−657.3	−618.0	−525.3

[a] RVS energy decomposition has been performed upon various extracted geometries in order to confirm the theoretical results on realistic systems. Thus, all the components, including water molecules, were taken into consideration. The number of water molecules is detailed for each complex, as well as the X-ray structure from which the system was extracted and the corresponding figure referenced. The same trend is observed, as for theoretical tetrahedral systems, concerning electrostatic energies favoring Mg(II) complexes, and the Ca(II) cation being more polarized, producing a greater charge transfer.

F Xa (1P0S) structure where the ω-loop is not formed. When only Ca(II) is present, the enzymatic activity is signicantly higher but can be enhanced by the addition of Mg(II). The three possible Mg(II) sites are constructed from three pairs of malonates provided by site no. 5 Gla16 and 26 (Gla17 and 27 for F IXa), site no. 7 Gla14 and 19 (Gla15 and 20 for FIXa), and site no. 9 Gla25 and 29 (Gla26 and 30 for F IXa). Close examination of these sites reveals that they all share the same pattern in which the cation is coordinated by two groups of two oxygens residing in the same side of two almost parallel malonate groups. Such geometry recalls the optimized geometry of the two malonates bound to a cation complex. Because they are not perfectly tetrahedral, these three binding sites will be called "deformed tetrahedral" cation binding sites. Figures 6a and b show ELF pictures of such a "deformed tetrahedral" binding site occupied by a Mg(II) cation as extracted from site no. 9 of F IXa (1J34) and a Ca(II) cation as extracted from site no. 7 of F Xa (1IOD), respectively. From Table 4, RVS total energies give the preferrence of Mg(II) over Ca(II) within this type of site by a difference of −109.4 kcal/mol for the optimized geometries and −91.1 for the extracted ones. This is due to the excess of first order energies in favor of Mg(II), namely, −89.4 and −76.5 kcal/mol. This is consistent with Mg(II) not splitting its subvalence and thus being involved in more electrostatic types of interactions. The presence of water molecules (two for Mg(II) and three for Ca(II)) within the coordination sphere of cations does not modify this conclusion (see Table 5).

The four other sites, however, are less structured, as their Ca(II) cations are coordinated four to eight times, in both monodentate and bidentate mode, by several carboxylate groups belonging to different Gla residues, as well as by carbonyl groups of the backbone of Ala1 (Tyr1 for F IXa) and the side chain of Asn2. For example, in site no. 6 of F IXa (1J34), Ca(II) is found octa coordinated, by Tyr1, Gla21 in a monodentate mode, Gla7 and -17 in a bidentate mode, and two water molecules (Figure 8b). The now familiar split of the subvalence of Ca(II) is observed. An ELF computation performed on this model reveals that the net charge of the cation within the system is +1.67 instead of +2 in the fundamental state. This means that up to one-third of an electron was transferred from the ligand oxygen lone pairs to the Ca(II) cation, with Ca(II) consistently able to adapt its electronic density to its environment by splitting its subvalence, thus entering into more covalent types of interactions. This capacity of adaptation for Ca(II) explains why, when only present in a coagulation factor environment, all the binding sites are loaded with Ca(II) (F VIIa 1DAN, F IXa 1J35, and F Xa 1IOD).

Therefore, with respect to the experimental results shown in Figure 5 of ref 2, a mechanism can be proposed for the activation of vitamin-K-dependent coagulation factors by Mg(II) and Ca(II) cations. Upon introducing first Mg(II) to a cation-free environment of an enzyme, one Mg(II) cation goes to each of the three "deformed tetrahedral" binding sites (nos. 5, 7, and 9), completing its coordination sphere with two water molecules. At this stage, the enzyme is not active and the ω-loop is not structured (F Xa 1P0S). When Ca(II) is added, one Ca(II) cation goes to each of the four other sites (nos. 3, 4, 6, and 8). This anchors Ala1 (or Tyr1 for F IXa) and Asn2 to the rest of the GLA domain[47] and folds the peptide in this particular ω geometry through interactions involving Gla6 and -7 (Gla7 and -8 for F IXa) and the rest of the domain (F VIIa 2A2Q). However, prepared with the same mix of cations at physiological concentration[39] as the one used to prepare F VIIa (2A2Q)[41] for the crystallization process, F IXa (1J34) exhibits a Ca(II) cation in central site no. 5 instead of a Mg(II) cation. Could the occupation of the central binding site no. 5 by either a Mg(II) (2A2Q) or a Ca(II) (1J34) be explained by the topological difference of the two cations?

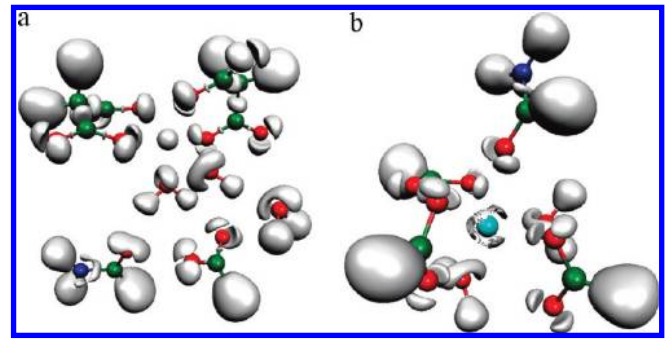

Figure 8. (a) Extracted geometry of binding site no. 5 of F VIIa (2A2Q) with Mg(II). (b) Extracted geometry of binding site no. 6 of F IXa (1J34) with Ca(II). Part a shows a tetrahedral binding site loaded with a Mg(II) cation, that structure being the ω-loop through a network of H-bonds established by highly polarized water molecules coordinated to the cation. Part b shows direct interactions between a Ca(II) cation and some constitutive segments of the ω-loop. The subvalence pattern of the two cations stays consistent with the one observed in all the studied geometries, whatever the size of the system considered.

c. Direct Interactions with Cations vs Interactions with Cations through Water. We consider here a system constituted by the five central Ca(II) binding sites extracted from the geometry of the GLA domain of F VIIa (1DAN), which is very similar to the one of F IXa (1J34). This complex was built from the backbone of Ala1, a formamide group representing the side chain of Asn2, and two malonates for Gla6 and -7, with Ala1, Asn2, Gla6, and Gla7 being part of the ω-loop, in addition to three malonate groups from Gla16, -20, and -26 and a formate given by Gla29 and the five Ca(II) ions. In addition, up to six water molecules were placed on the calcium ions according to their position in the X-ray structure. This system, which is globally neutral, is an X-ray crystal snapshot where hydrogens and waters have been added, focusing on the interactions between Ca(II) cations and their ligands. Such a system is found in X-ray crystal structures 1DAN, 1J34, 1J35, and 1IOD in which cations directly interact with their environment. Figure 9 exhibits the ELF study on this system. This picture reveals the network of interactions between the subvalence basins of the cations and the lone pairs of the coordinating oxygens. The split of all Ca(II) subvalences indicates that these interactions are partially covalent because they are built from electronic exchanges between the cations and the lone pairs present in their immediate environment. This results in a

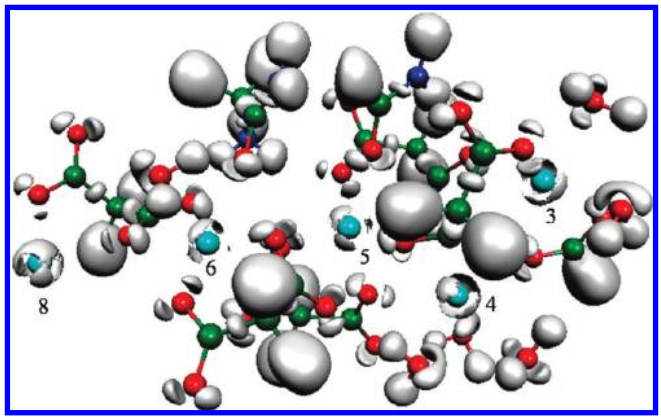

Figure 9. Topological analysis of the five central Ca(II) binding sites of F VIIa (1DAN) GLA domain. This picture unravels the network of charge transfer interactions between the five Ca(II) cations and the oxygen lone pairs borne by Gla residues of the two upper α-helices, on one hand, and the oxygen lone pairs borne by Ala1 (backbone), Asn2 (side chain), and Gla6 and -7 of the lower ω-loop, on the other hand. These interactions structure the ω-loop in its functional geometry. It can be noticed that Ca(II) cations show different patterns of their subvalence split according to their different numbers of coordinaton. The numbering of the calcium ion binding sites of Figure 3 is used.

network of many-body interactions at the center of the GLA domain. QTAIM values of M_1 of each Ca(II), computed with the ELF function, confirm the intensity of the charge transfer. Ca(II) no. 3 and 5, each being 7-fold coordinated, have the lowest value of the series with a M_1 value of 0.041 D and a net charge of +1.66 instead of +2, whereas Ca(II) no. 4 and 6, with 6-fold coordination, exhibit enhanced values, namely, 0.060 D and +1.68, for M_1 and the charge, respectively. Ca(II) no. 8, being four times coordinated, shows values of M_1 very close (0.166 D, +1.72) to the one found for the small bidentate formate−cation complex (0.160 D and +1.70 for M_1 and the charge, respectively, see Table 1). This indicates that the greater the coordination number, the less the polarization and therefore the residual charge.

In the GLA domain of F VIIa (2A2Q), the central Mg(II) is found six times coordinated: four times tetrahedrally by malonates of Gla16 and -26 and two times by water molecules S209 and S363 (Figure 8a). The formamide moiety of Asn2, a formate group from Gla7, and a third water complete the network of H-bonds through which this central Mg(II) contributes to structure the ω-loop. As seen in Figure 8a, the central Mg(II) subvalence remains almost perfectly spherical, as in the bidentate formate−Mg(II) complex and in the two-malonate−Mg(II) tetrahedral optimized geometry. Close examination of the RVS polarization contribution (Table 5) reveals that, if the cation is as expected almost not polarized, the polarization of the three water molecules accounts for approximately 30% of the total polarization of −92.7 kcal/mol. Indeed, one of the water molecules is highly polarized and bears an Epol(RVS) value of −13.9 kcal/mol. Thus, interactions between the cation and the ω-loop are established through highly polarized water molecules.

While the presence of Ca(II) is required[2,3,48] in the central region for an effective coagulation function, it has been demonstrated that the affinity of coagulation factors for either cellular membranes,[45,49] tissue factors,[5] or anticoagulant agents[36,40] is strongly enhanced when external sites are occupied by Mg(II).[40] This supports our findings that these sites are better stabilized by Mg(II)[37] rather than Ca(II).

Therefore, the difference of the two geometries (1J34 and 2A2Q) resides in the fact that, in 2A2Q, the central site is occupied by a Mg(II) which is only able to complete its coordination shell with water, for which the residence time has been measured to be on the order of 1 μs.[8] This explains the greater distance between the two α-helices and the ω-loop (2A2Q case), namely, the interposition of a water layer. Therefore, one of the roles of the cations is to fix water, which in turn binds to the ω-loop through a network of H-bonds. By contrast, in FIXa 1J34, where all the central cation binding sites are occupied by Ca(II), interactions take place directly between metal cations and the lone pairs borne by its ligating oxygens. In this connection, it was recently demonstrated that water layers present either between separate domains of a protein or in between different proteins are in dynamic short time exchanges with the solvation water present in the environment.[50,51] Therefore, it is possible to make the hypothesis that F VIIa crystallized by Bajaj et al. (2A2Q), with interactions through water (i.e., water mediated interactions), could be present, free in the blood plasma since the latter is a highly hydrophilic environment. On the other hand, the GLA domain of F IXa crystallized by Shikamoto et al. (1J34) is found bound to a ligand (in this case, a snake venom protein); this binding could impose the "direct interactions with cations" geometry. It is, then, perhaps reasonable to suggest that this is the geometry that inserts deeply into the cell membrane, the interior of which is a highly hydrophobic environment. Indeed, the insertion within the membrane may expel water molecules from the inserted part of the GLA domain, imposing a switch between "physics at play": going from a "through water structure" to a "direct electronic interactions structure".

Conclusion

In this contribution, we have used several theoretical tools to illustrate the relationship between the electronic structure of selected metal−cation complexes and the so-called hard and soft chemical behavior. The ELF analysis allows ranking cations according to their topological signature, namely, their ability to split their valence into subdomains (subvalent basins). Hard cations will not exhibit such a capability as soft cations do. The covalent character of the ligand−metal cation interaction is associated with a basin between the metal and the neighboring heavy atoms. That way, such a covalent interaction can be directly affected by the cations' environment, and as we have seen, an electrostatic interaction, as in Mg(II) monodentate-like complexes, can become covalent, exhibiting an extra subvalent localization basin under specific stress conditions. This topological metal cation ranking has been shown to be relevant when compared to RVS and CSOV energy analyses, as well as in good qualitative

agreement with local Fukui functions extracted from both QTAIM and ELF analyses.

Our integrated methodological approach uncovered a clear relationship between the underlying metal electron structure and the biological activity of enzymes such as vitamin-K-dependent coagulation factors. The present approach could then be extended to other biological systems involving metal cations. It is also important to point out that these results on metal cation−ligand complexes, such as the dissymmetry between internal and external carboxylate oxygen lone pairs, could also provide useful information for the design of new force fields.[7a,52] Moreover, applications to the problem of blood coagulation allowed us to address the Ca(II) vs Mg(II) selectivity in their interaction with GLA domains. Only the two X-ray structures, crystallized using the same Mg(II)/Ca(II) mix found under physiological conditions (1J34 and 2A2Q), have been investigated.

In the first one (1J34), Ca(II) has been shown to be more covalently bonded to ligand than Mg(II), enabling the creation of a "direct charge transfer network" between its subvalence and the carboxylate oxygen lone pairs. We showed that this concept could also uncover the distinct role of the two cation binding sites present in GLA domains. Being at the origin of the observed charge transfer network, calcium cations are mandatory in the central region to conserve the folding, whereas external binding sites are better stabilized by Mg(II), in agreement with the experiment, thanks to strong electrostatic interactions with the environment.

In the second structure (2A2Q), in which some interactions between metal cations and Gla are established through the presence of crystallized water molecules, we have shown that magnesium is able to form "an indirect charge transfer network" with malonates through its interaction with two highly polarized water molecules that are responsible for a structure of the ω-loop similar to that observed in the first structure (1J34). To conclude, as the two crystal structures have been solved, they could be the two interconverting forms of the same system, each of them having a different water requirement. In both cases, the ω-loop is present. This is required for the active enzyme, but the underlying physics is not the same. In the first structure, the folding is mainly due to electronic effects: Ca(II) is preferred in the five central binding sites. By contrast, the presence of water molecules is able to reverse the direct electronic selectivity of cations (Mg(II) could be present if interacting with two water molecules). This clearly indicates that dynamical solvent effects could play a key role in the observed structure of the domain. The connection between the two structures might be established through a series of molecular dynamics simulations. This work also emphasizes again[53] the importance of a "discrete" water molecule to understand the stability of biological systems, as the presence of a limited number of structured water molecules could be critical to obtain meaningful theoretical models.

Acknowledgment. The computations have been performed at the national IDRIS (F. 91403 Orsay, France), CRIHAN (F.76800 Saint-Etienne-du-Rouvray, France), and CINES (F. 34097 Montpellier, France) supercomputing centers. Some ELF computations have been run at the local CCRE centre at Université Pierre et Marie Curie, Univ Paris 6 (F. 75252 Paris CEDEX 05, France). Support from the French National Research Agency (ANR) on project LASIHMODo (BLAN08-3_312754) is acknowledged. This research was supported in part by the Intramural Research program of the NIH and NIEHS.

Supporting Information Available: (S1) Performance of the B3LYP functional. (S2) Effects of PCM solvation over the topology of two bidentate formate-cation complexes. (S3) CSOV computations (DFT level). This information is available free of charge via the Internet at http://pubs.acs.org/.

References

(1) Furie, B.; Furie, B. C. *Cell* **1988**, *53*, 505–518.

(2) Prendergast, F. G.; Mann, K. G. *J. Biol. Chem.* **1977**, *252*, 840–850.

(3) van den Besselaar, A. M. H. P. *Blood Coagulation Fibrinolysis* **2002**, *13*, 19–23.

(4) Wang, S. X.; Hur, E.; Sousa, C. A.; Brinen, L.; Slivka, E. J.; Fletterick, R. J. *Biochemistry* **2003**, *42*, 7959–7966.

(5) Persson, E.; Ostergaard, A. *J. Tromb. Haemost.* **2007**, *5*, 1977–1978.

(6) (a) Lightstone, F. C.; Schwegler, E.; Hood, R. Q.; Gygi, F.; Galli, G. *Chem. Phys. Lett.* **2001**, *343*, 549–555. (b) Naor, M. M.; Van Nostrand, K.; Dellago, C. *Chem. Phys. Lett.* **2003**, *369*, 159–164. (c) Bako, I.; Hutter, J.; Palinkas, G. *J. Chem. Phys.* **2002**, *117*, 9838–9843. (d) Lightstone, F. C.; Schwegler, E.; Allesch, M.; Gygi, F.; Galli, G. *Chem. Phys. Chem.* **2005**, *6*, 1745–1749.

(7) (a) Piquemal, J.-P.; Perera, L.; Cisneros, G. A.; Ren, P.; Pedersen, L. G.; Darden, T. A. *J. Chem. Phys.* **2006**, *125*, 054511−1-7. (b) Babu, C. S.; Lim, C. *J. Phys. Chem. A* **2006**, *110*, 691–699.

(8) Neely, J.; Connick, R. *J. Am. Chem. Soc.* **1970**, *92*, 3476–3478.

(9) (a) Bader, R. F. W. *Atoms In Molecules: A Quantum Theory*; Oxford University Press: Oxford, U. K., 1990. (b) Matta, C. F.; Boyd, R. J. *The Quantum Theory of Atoms in Molecules: From Solid State to DNA and Drug Design*; Wiley-VCH: Weinheim, Germany, 2007. (c) Popelier, P. L. A. *Atoms In Molecules: An Introduction*; Prentice-Hall: Harlow, U. K., 2000.

(10) (a) Becke, A. D.; Edgecombe, K. E. *J. Chem. Phys.* **1990**, *92*, 5397–5403. (b) Silvi, B.; Savin, A. *Nature (London)* **1994**, *371*, 683–686.

(11) (a) Stevens, W. J.; Fink, W. *Chem. Phys. Lett.* **1987**, *139*, 15–22. (b) Bagus, P. S.; Illas, F. *J. Chem. Phys.* **1992**, *96*, 8962–8970.

(12) Silvi, B.; Fourré, I.; Alikani, M. E. *Chemie* **2005**, *136*, 855–879.

(13) Silvi, B. *J. Phys. Chem. A* **2003**, *107*, 3081–3085.

(14) Martín Pendás, A.; Francisco, E.; Blanco, M. A. *Chem. Phys. Lett.* **2008**, *454*, 396–403.

(15) (a) Gillespie, R. J.; Popelier, P. L. A. *Chemical Bonding and Molecular Geometry*; Oxford University Press: Oxford U. K., 2001. (b) Gillespie, R. J.; Robinson, E. A. *J. Comput. Chem.* **2007**, *34*, 396–407.

(16) Gillespie, R. J.; Noury, S.; Pilme, J.; Silvi, B. *Inorg. Chem.* **2004**, *43*, 3248–3256.

(17) Piquemal, J.-P.; Pilmé, J.; Parisel, O.; Gérard, H.; Fourré, I.; Bergès, J.; Gourlaouen, C.; de la Lande, A.; van Severen, M. C.; Silvi, B. *Int. J. Quantum Chem.* **2008**, *108*, 1951–1969.

(18) (a) Pilmé, J.; Piquemal, J.-P. *J. Comput. Chem.* **2008**, *29*, 1440–1449. (b) Fukui, K.; Yonezawa, T.; Shingu, H. *J. Chem. Phys.* **1952**, *20*, 722–725. Fukui, K.; Yonezawa, T.; Nagata, C.; Shingu, H. *J. Chem. Phys.* **1954**, *22*, 1433–1442. (c) Woodward, R. B.; Hoffmann, R. *The Conservation of Orbital Symmetry*; Chemie: Weinheim, Germany, 1970. (d) Parr, R. G.; Yang, W. *Density Functional Theory of Atoms and Molecules*; Oxford University Press: New York, 1989. (e) Morell, C.; Grand, A.; Toro-Labbé, A. *J. Phys. Chem. A* **2005**, *109*, 205–212. (f) Morell, C.; Grand, A.; Toro-Labbé, A. *Chem. Phys. Lett.* **2006**, *425*, 342–346. (g) Cioslowski, J.; Martinov, M.; Mixon, S. T. *J. Phys. Chem.* **1993**, *97*, 10948–10951. (h) Contreras, R. R.; Fuentealba, P.; Galván, M.; Pérez, P. *Chem. Phys. Lett.* **1999**, *304*, 405–413. (i) Bulat, F. A.; Chamorro, E.; Fuentealba, P.; Toro-Labbé, A. *J. Phys. Chem. A* **2004**, *108*, 342–349. (j) Tiznado, W.; Chamorro, E.; Contreras, R.; Fuentealba, P. *J. Phys. Chem. A* **2005**, *109*, 3220–3224.

(19) (a) Lee, C.; Yang, W.; Parr, R. G. *Phys. Rev. B* **1988**, *37*, 785–789. (b) Becke, A. D. *J. Chem. Phys.* **1993**, *98*, 5648–5652. (c) Burda, J. V.; Šponer, J.; Hobza, P. J. *J. Phys. Chem.* **1996**, *100*, 7250–7256. (d) Russo, N.; Toscano, M.; Grand, A. *J. Phys. Chem. A* **2003**, *107*, 11533–11538.

(20) *Jaguar 6.5*; Schrodinger Inc.: Portland, OR, 2005.

(21) Hay, P. J.; Wadt, W. R. *J. Chem. Phys.* **1985**, *82*, 299–310.

(22) Krishnan, R.; Binkley, J. S.; Seeger, R.; Pople, J. A. *J. Chem. Phys.* **1980**, *72*, 650–654.

(23) Frisch, M. J.; Trucks, G. W.; Schlegel, H. B.; Scuseria, G. E.; Robb, M. A.; Cheeseman, J. R.; Montgomery, J. J. A.; Vreven, T.; Kudin, K. N.; Burant, J. C.; Millam, J. M.; Iyengar, S. S.; Tomasi, J.; Barone, V.; Mennucci, B.; Cossi, M.; Scalmani, G.; Rega, N.; Petersson, G. A.; Nakatsuji, H.; Hada, M.; Ehara, M.; Toyota, K.; Fukuda, R.; Hasegawa, J.; Ishida, M.; Nakajima, T.; Honda, Y.; Kitao, O.; Nakai, H.; Klene, M.; Li, X.; Knox, J. E.; Hratchian, H. P.; Cross, J. B.; Bakken, V.; Adamo, C.; Jaramillo, J.; Gomperts, R.; Stratmann, R. E.; Yazyev, O.; Austin, A. J.; Cammi, R.; Pomelli, C.; Ochterski, J. W.; Ayala, P. Y.; Morokuma, K.; Voth, G. A.; Salvador, P.; Dannenberg, J. J.; Zakrzewski, V. G.; Dapprich, S.; Daniels, A. D.; Strain, M. C.; Farkas, O.; Malick, D. K.; Rabuck, A. D.; Raghavachari, K.; Foresman, J. B.; Ortiz, J. V.; Cui, Q.; Baboul, A. G.; Clifford, S.; Cioslowski, J.; Stefanov, B. B.; Liu, G.; Liashenko, A.; Piskorz, P.; Komaromi, I.; Martin, R. L.; Fox, D. J.; Keith, T.; Al-Laham, M. A.; Peng, C. Y.; Nanayakkara, A.; Challacombe, M.; Gill, P. M. W.; Johnson, B.; Chen, W.; Wong, M. W.; Gonzalez, C.; Pople, J. A. *Gaussian 03*, Revision C.02; Gaussian Inc.: Wallingford, CT, 2007.

(24) Noury, S.; Krokidis, X.; Fuster, F.; Silvi, B. *J. Comput. Chem.* **1999**, *23*, 597–604. The modified TopMod90 program (named TopChem) is available upon request. See the following Web site for details http://www.lct.jussieu.fr/pagesperso/pilme (accessed 01/15/2010).

(25) Piquemal, J.-P.; Marquez, A.; Parisel, O.; Giessner-Prettre, C. *J. Comput. Chem.* **2005**, *26*, 1052–1062.

(26) Schmidt, M. W.; Baldridge, K. K.; Boatz, J. A.; Elbert, S. T.; Gordon, M. S.; Jensen, J. H.; Koseki, S.; Matsunaga, N.; Nguyen, K. A.; Su, S.; Windus, T. L.; Dupuis, M.; Montgomery Jr, J. A. *J. Comput. Chem.* **1993**, *14*, 1347–1363.

(27) Ratcliffe, J. V.; Furie, B.; Furie, B. C. *J. Biol. Chem.* **1993**, *268*, 24339–24345.

(28) de Courcy, B.; Gresh, N.; Piquemal, J.-P. *Interdiscip. Sci. Comput. Life Sci.* **2009**, *1*, 55–60.

(29) Parr, R. G.; Pearson, R. G. *J. Am. Chem. Soc.* **1983**, *105*, 7512–7516.

(30) Xu, X.; Zhang, L.; Shen, D.; Wu, H.; Peng, L.; Li, J. *J. Biol. Inorg. Chem.* **2009**, *14*, 559–571.

(31) Perera, L.; Foley, C.; Darden, T. A.; Stafford, D.; Mather, T.; Esmon, C. T.; Pedersen, L. G. *Biophys. J.* **2000**, *79*, 2925–2643.

(32) Hoffman, M. *J. Thromb. Thrombolysis* **2003**, *16*, 17–20.

(33) Roberts, H. R.; Hoffman, M.; Monroe, D. M. *Semin. Thromb. Hemost.* **2006**, *32* (Suppl. 1), 32–38.

(34) McDonald, J. F.; Shah, A. M.; Schwalbe, R. A.; Kisiel, W.; Dahlbäck, B.; Nelsestuen, G. L. *Biochemistry* **1997**, *36*, 5120–5127.

(35) Soriano-Garcia, M.; Padmanabhan, K.; de Vos, A. M.; Tulinsky, A. *Biochemistry* **1992**, *31*, 2554–2566.

(36) Gopinath, S. C. B.; Shikamoto, Y.; Mizuno, H.; Kumar, P. K. R. *Biochem. J.* **2007**, *405*, 351–357.

(37) Sekiya, F.; Yamashita, T.; Atoda, H.; Komiyama, Y.; Morita, T. *J. Biol. Chem.* **1995**, *270*, 14325–14331.

(38) Banner, D. W.; D'Arcy, A.; Chene, C.; Winkler, F. K.; Guha, A.; Konigsberg, W. H.; Nemerson, Y.; Kirchhofer, D. *Nature (London)* **1996**, *380*, 41–46.

(39) Shikamoto, Y.; Morita, T.; Fujimoto, Z.; Mizuno, H. *J. Biol. Chem.* **2003**, *278*, 24090–24094.

(40) Mizuno, H.; Fujimoto, Z.; Atoda, H.; Morita, T. *Proc. Natl. Acad. Sci. U.S.A.* **2001**, *98*, 7230–7234.

(41) Bajaj, S. P.; Schmidt, A. E.; Agah, S.; Bajaj, M. S.; Padmanabhan, K. *J. Biol. Chem.* **2006**, *281*, 24873–24888.

(42) Falls, L. A.; Furie, B. C.; Jacobs, M.; Furie, B.; Rigby, A. C. *J. Biol. Chem.* **2001**, *276*, 23895–23902.

(43) Ohbuko, Y. Z.; Tajkhorshid, E. *Structure* **2008**, *16*, 72–81.

(44) Sunnerhagen, M.; Forsén, S.; Hoffrén, A.-M.; Drakenberg, T.; Teleman, O.; Stenflo, J. *Nat. Struct. Biol.* **1995**, *2*, 504–509.

(45) Taboureau, O.; Olsen, O. H. *Eur. Biophys. J.* **2007**, *36*, 133–144.

(46) Davis, C. H.; Deerfield, D., II; Stafford, D. W.; Pedersen, L. G. *J. Phys. Chem. A* **2007**, *111*, 7257–7261.

(47) Huang, M.; Furie, B. C.; Furie, B. *J. Biol. Chem.* **2004**, *279*, 14338–14346.

(48) Huang, M.; Rigby, A. C.; Morelli, X.; Grant, M. A.; Huang, G.; Furie, B.; Seaton, B.; Furie, B. C. *Nat. Struct. Biol.* **2003**, *10*, 751–756.

(49) Sekiya, F.; Yoshida, M.; Yamashita, T.; Morita, T. *J. Biol. Chem.* **1996**, *271*, 8541–8544.

(50) Lin, J.; Balabin, I. A.; Beratan, D. N. *Science* **2005**, *310*, 1311–1313.

(51) de La Lande, A.; Marti, S.; Parisel, O.; Moliner, V. *J. Am. Chem. Soc.* **2007**, *129*, 11700–11707.

(52) (a) Gresh, N.; Cisneros, G. A.; Darden, T. A.; Piquemal, J.-P. *J. Chem. Theory Comput.* **2007**, *3*, 1960–1986. (b) Piquemal, J.-P.; Chevreau, H.; Gresh, N. *J. Chem. Theory Comput.* **2007**, *3*, 824–837. (c) Piquemal, J.-P.; Cisneros, G. A.; Reinhardt, P.; Gresh, N.; Darden, T. A. *J. Chem. Phys.* **2006**, *124*, 104101−1-12.

(53) de Courcy, B.; Piquemal, J.-P.; Garbay, C.; Gresh, N. *J. Am. Chem. Soc.* **2010**, *132*, 3312−3320.

CT100089S